

Incorporating Optimal Operation Strategies into Investment Planning for Wind/Electrolyser System

Yi Zheng[✉], Shi You, Henrik W. Bindner, and Marie Münster

Abstract—As a conducive and prevalent technique for producing green hydrogen, hybrid wind-based electrolyzer system requires both effective planning and operation to realize its techno-economic value. Majority of the existing studies are focused on either of these two, but none of them sufficiently emphasize on their interrelationship. In this paper, we propose a two-stage multi-objective optimization framework to reveal optimal investment plans considering various operational strategies, such as economic revenue maximization and green hydrogen production maximization. The results reveal that: 1) A trade-off exists between system investment and the capacity to accomplish optimal operational performance. For example, the system demands flexibility to boost operational profits, but this results in high investment costs. 2) Differentiated operation objectives generate different component capacities during the planning phase. 3) Regarding a wind-hydrogen system with gas storage, the Pareto optimal design manifesting the trade-off between system investment and prime operational performance can be actualized along the margins of a feasible solution.

Index Terms—Hybrid wind-hydrogen system, multi-objective optimization, optimal operation, planning, sizing.

NOMENCLATURE

A. Abbreviations

HWHS	Hybrid wind hydrogen system.
AEL	Alkaline electrolyser.
PEM	Proton exchange membrane electrolyser.
SOEC	Solid oxide electrolyser.
IRR	Internal rate of return.
NPV	Net present value.
NPC	Net present cost.
RLU	Upward ramping rate limit.
RLD	Downward ramping rate limit.
GLS	GreenLab Skive.

Manuscript received June 2, 2021; revised October 12, 2021; accepted January 6, 2022. Date of online publication February 14, 2022; date of current version February 21, 2022. This work was supported by the European Union's Horizon 2020 research and innovation programme under grant agreement No. 775970.

Y. Zheng (ORCID: <https://orcid.org/0000-0002-6116-4055>), S. You (corresponding author, email: sy@elektro.dtu.dk), and H. W. Bindner are with the Department of Electrical Engineering, Technical University of Denmark, 2800 Kgs. Lyngby, Denmark.

M. Münster is with the Department of Technology, Management and Economics, Technical University of Denmark, 2800 Kgs. Lyngby, Denmark.
DOI: 10.17775/CSEEJPES.2021.04240

I. INTRODUCTION

Hydrogen is perceived as a promising energy carrier in the future energy system mainly due to its intrinsic green properties and wide use as feedstocks across many industries [1]. However, most of the hydrogen used currently is derived from the reforming of methane, and hence, does not fully qualify as a non-polluting or clean energy [2]. Green hydrogen, also referred to as clean hydrogen, therefore, has gained considerable attention in recent years. It refers to hydrogen produced by pure renewable energy sources without releasing any CO₂ during its total life cycle. Wind energy and solar energy are primary renewable sources used for producing green hydrogen and the former accounts for the greater share of the interest [3]–[5]. Numerous projects and studies on hybrid wind hydrogen system (HWHS) have been performed all around the world. These projects mainly focus on system configuration, demonstration, and techno-economic analysis to demonstrate the feasibility of the said green hydrogen production pathway.

HWHSs can be categorized into off-grid and on-grid ones. Certain studies concentrate on the off-grid configuration in rural areas considering its profitability of producing green hydrogen [6], [7]. The associated long-term sizing and planning problems are also investigated [8]. For an on-grid system, inclusion of the power grid significantly affects the system performance, creating both new opportunities as well as challenges. For example, electrolysers can be scheduled to perform energy arbitrage in power markets [9], thereby reducing operational costs. It is widely believed that the usage of flexibility in such HWHS could effectively reduce the cost of green hydrogen [10].

Particularly considering an on-grid HWHS, the design, operation, and other associated optimizations form the pivotal concerns that have been extensively evaluated. Certain studies investigate the operational strategies of such systems very closely, that is, given a pre-specified system, developing a strategy to achieve certain objectives by controlling/scheduling/dispatching related energy components. Gruger *et al.* proposed an optimal electrolyzer operation to reduce possible costs in the presence of constraints of hydrogen demand [11]. Akbar adopted meta-heuristic approaches to optimize the operation of a grid-connected hybrid solar-wind-hydrogen CHP system. The objective was to minimize the operation and maintenance cost of this system [12]. Other papers, from another point of view, aim at offering an optimal sizing to reach maximal yearly benefits under different scenar-

ios [6], [13], [14]. However, in such studies, the design and operational optimization usually exist as isolated attributes, which means one of them remains fixed while the other one is optimized.

Hence, some researchers try to take both of them into account simultaneously. A general idea is to view the planning as the first stage, followed by operation. For example, for the framework of two-stage stochastic programming, the planning variables, i.e., the installed capacity and the number of units to be deployed, are called “here and now,” while the operation variables, such as hydrogen production rate, are called “wait and see” [15]. The planning decisions need to be determined before the realization of uncertain parameters, while the operation decisions can be taken after these parameters are revealed. These two-stage methods are mature and widely used [16], [17]. The formulated optimization could either be solved by analytic approaches [18] (mostly mixed linear programming) or by heuristic algorithms [19]. Nonetheless, valuable improvements have been made with respect to this classical problem. First, the utilized models of the most important component, electrolyzers, are generally based on a constant efficiency assumption and are not fully validated. Second, these two-stage approaches primarily aim for a single objective—by and large, economic benefit maximization and strongly interfused planning and operation, signifying the overall rigidity of the framework. When the operation objective changes, the problem needs to be recreated in a holistic manner.

To bridge this gap, in this paper, we concentrate on a typical HWHS system and offer a flexible multi-objective two-stage optimization considering both planning and operation. A first principle-based electrolyser model is established. This model is able to reveal the non-linear relation between hydrogen production and power input, which improves the accuracy compared to those based on linear assumption [12], [20], [21]. Furthermore, a two-stage hybrid optimization is proposed, in which the inner optimization (inner loop) determines the optimal operational strategies while the outer optimization sheds light upon the system planning, i.e., the investment decisions. The two-stage optimization strategy is easily extensible and can be adopted for analyzing multiple combinations of investment planning and operational objectives. Furthermore, the proposed method is implemented in a live industrial park-GreenLab Skive in Denmark- to validate the feasibility and provide suggestions to relevant stakeholders.

This paper is organized as follows: Section I provides a brief introduction of state-of-the-art research on HWHS, followed by section II that introduces how the involved components are modelled. A detailed alkaline electrolyser model is described in this part. In section III, we propose a two-stage optimization scheme that is utilized in this research. The formulation of this hybrid optimization problem is also described in this section. Afterwards, a case study on the real-life industrial park is studied in detail to test the proposed method. In section V, we illustrate the optimal operation of the electrolyser with respect to different operational objectives, i.e., economic revenue maximization and green hydrogen production maximization. We further discuss the influence of planning on

the optimal operation from the perspective of sensitivity and Pareto optimum. Section VI concludes this study.

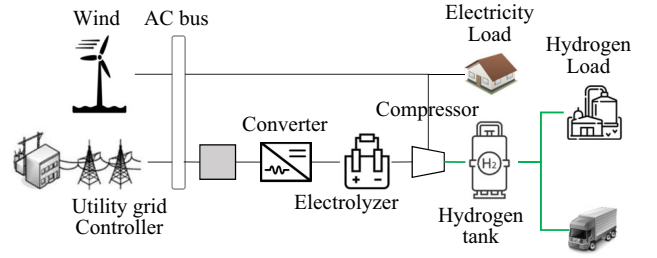


Fig. 1. Schematics for hybrid wind-hydrogen system.

II. SYSTEM MODELING

A. Wind Energy Conversion System

The power output of a wind turbine is formulated as in [22]:

$$P_w(t) = \begin{cases} 0, & v < v_{ci} \\ P_f(v), & v_{ci} \leq v < v_r \\ P_r, & v_r \leq v < v_{co} \\ 0, & v_{co} \leq v \end{cases} \quad (1)$$

where v_{ci} denotes the cut-in speed (m/s), v_{co} is the cut-out speed (m/s) and v_r is the rated speed (m/s). The wind speed v (m/s) in this equation is the one at the height of blades, but wind speed is commonly measured near the ground. The link between wind speed and height is exhibited as:

$$\left(\frac{v_2}{v_1}\right) = \left(\frac{h_2}{h_1}\right)^\alpha \quad (2)$$

where v_1 is the wind speed (m/s) at the reference height h_1 (m) and v_2 (m/s) is the speed at the height h_2 (m). α is the Hellman coefficient describing the surface roughness which varies from 0.128 to 0.160 [23]. $P_f(v)$ is given by the cubic law as:

$$P_f(v) = \frac{1}{2} \rho A C_p v^3 \quad (3)$$

where ρ is the air density at the hub height (kg/m^3) and C_p is the power coefficient of wind turbine, which is estimated to be 0.42 based on [24].

B. Electrolyser

In the studied system, an alkaline electrolyser (AEL) is used to produce hydrogen. There are currently three electrolysis technologies available: AEL, proton exchange membrane electrolyser (PEM) and solid oxide electrolyser (SOEC). SOEC bears the highest theoretical efficiency but is not yet applicable to large scale applications. AEL and PEM are both well-developed and have high technology maturity [4]. PEM has exhibited better flexibility when it comes to transient operation (feasible load range, start-up time and stand-by lost) [25]. Nevertheless, the investment and lifetime are dominant factors in the market, which makes AEL more conducive for large-scale applications [26]. An analytic model is established to describe the typical polarization curve based on physical

laws. The polarization curve, also known as the I-V curve is formulated as in [27]:

$$E_{\text{cell}} = E_{\text{rev}} + E_{\text{act}} + E_{\text{ohm}} + E_{\text{diff}} \quad (4)$$

where E_{cell} is the voltage of electrolyser (V), and E_{rev} is the open-circuit voltage (V), the theoretical minimum voltage that allows water dissociation reaction. $E_{\text{act}}, E_{\text{ohm}}, E_{\text{diff}}$ are overvoltage (V) dominated by different irreversible physical processes. E_{rev} is formulated by:

$$E_{\text{rev}} = E_{\text{rev}}^0 + \frac{RT}{2F} \ln \left(\frac{P_{\text{H}_2} \sqrt{P_{\text{O}_2}}}{a_{\text{H}_2\text{O}}} \right) \quad (5)$$

where with E_{rev}^0 is the reversible voltage in standard condition (V), varying with temperature T . The correlation can be expressed empirically, as shown in (6) [24]. For a hydrogen and oxygen system, at 293.15K, the E_{rev}^0 is 1.229V.

$$E_{\text{rev}}^0(T) = 1.5184 - 1.5421 \times 10^{-3}T + 9.523 \times 10^{-5}T \ln(T) + 9.84 \times 10^{-8}T^2 \quad (6)$$

The second part in (5) describes the deviation from the standard condition, where R is the gas constant (J/(mol K)), F the Faraday constant (C/mol) and $a_{\text{H}_2\text{O}}$ the thermal dynamic activity of water (mol/m³).

Activation overvoltage E_{act} , caused by the activation energy barrier of electrode reactions, is described by the Butler-Volmer equation that is formulated as:

$$I = I_{0,k} \left[\exp \left(\frac{\alpha_k z F E_{\text{act},k}}{RT} \right) - \exp \left(-\frac{(1 - \alpha_k) z F E_{\text{act},k}}{RT} \right) \right] \quad (7)$$

where I is the electrolyser current density (A/m²), $I_{0,k}$ is the exchange current density (A/m²), and α_k is the charge transfer coefficient that describes the influence of electrode potential on oxidation and reduction reaction. This transcendental equation is usually replaced by its simplified forms such as Tafel or symmetric equation. In this study, it is directly solved by using the Newton's method.

Ohmic overvoltage describes the resistance from different parts of an electrolyser covering electrode, electrolyte, bipolar plates, etc. Since the resistance from electrolyte is the decisive factor, other resistances are neglected in this study. Ohmic voltage is calculated as:

$$E_{\text{ohm}} = \frac{IL}{\sigma} \quad (8)$$

where L is the thickness of electrolyte (cm) and σ is the specific electrolyte conductivity (S/cm), which is presented as in [28]:

$$\begin{aligned} \sigma = & 0.279844 \times (100w) - 0.009241 \times T - 0.000149 \times T^2 \\ & - 0.000905 \times (100w) \times T \\ & + 0.000114 \times T^2 \times (100w)^{0.1765} \\ & + 0.069664 \times T / (100w) - 28.9815 \times (100w) / T \end{aligned} \quad (9)$$

Here, $100w$ denotes the mass fraction of potassium hydroxide. This nonlinear regression has been validated with experimental data and the correlation coefficient (R^2) could reach up to 0.999.

Diffusion overvoltage is the main loss of the electrolyser in high current density. In this situation, the system reaction is not limited by charge transfer but is dominated by mass transfer. By introducing the limited current density I_{lim} (A/m²), the diffusion overvoltage can be expressed as (with β as the empirical coefficient):

$$E_{\text{diff}} = \frac{RT}{2\beta F} \ln \left(1 + \frac{I}{I_{\text{lim}}} \right) \quad (10)$$

To obtain the hydrogen production rate, Faraday Law is used to connect the current density I and hydrogen production rate \dot{n}_{H_2} (mol/s):

$$\dot{n}_{\text{H}_2} = \frac{\eta_F n_C I A}{2F} \quad (11)$$

where η_F is the Faraday efficiency, and F is Faraday constant. This efficiency is also called as current efficiency, since it is triggered by parasitic current losses along the gas ducts. The parasitic currents rise with decreasing current density. An empirical expression is given in (12) [29], which can accurately estimate the relationship between Faraday efficiency and current density. n_C stands for the number of cells in series and A is the cell area (m²).

$$\eta_F = \frac{I^2}{f_1 + I^2} f_2 \quad (12)$$

with f_1, f_2 as two constant values. To use this equation, the unit of I should be (mA/cm²), whereas in other equations it is (A/m²). When the current density is large enough, η_F approaches one, indicating that the relationship of the electrolyser input power and hydrogen production is almost linear. However, the existence of Faraday efficiency makes the efficiency curve of the electrolyser nonlinear. The efficiency is defined as follows, where HHV is the high heat value of hydrogen (J/mol) and P_{ele} the power (W):

$$\eta_{\text{ele}} = \frac{\dot{n}_{\text{H}_2} \text{HHV}}{P_{\text{ele}}} \quad (13)$$

$$P_{\text{ele}} = I A E_{\text{cell}} \quad (14)$$

The efficiency and production curves for an electrolyser cell are shown in Fig. 2, where the former exhibits strong non-linearity. With lower working temperature, the non-linearity is enhanced. To further guarantee the accuracy of this model, we compared the simulation results with real experiment data from studies at different temperature and varying current loads (see Fig. 3). By and large, the model successfully describes the relationship between power demand and current loads. The way the temperature affects the electrolyser behavior is also incorporated in this model. It is also observed that under lower current densities, this model tends to be less accurate, but since an alkaline electrolyser is typically operated at comparatively high current density to avoid any instabilities, these deviations are accepted.

C. Compressor

Since hydrogen is usually utilized (e.g. methanol synthesis) and transported under high pressure (via trailers), it is crucial to compress hydrogen before utilization. If the compression

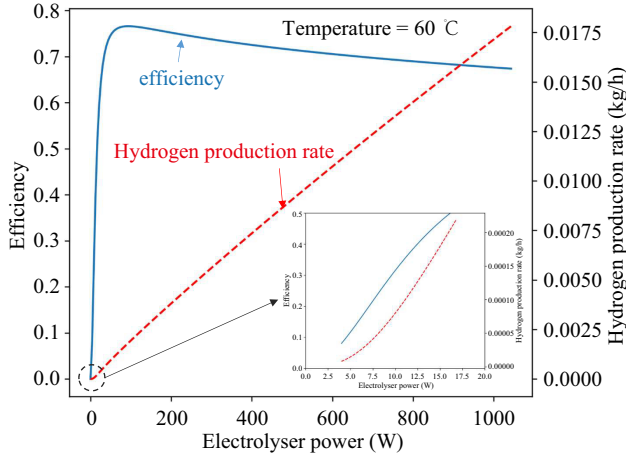


Fig. 2. Electrolyser efficiency and hydrogen production rate as functions of input power. The sub-figure reveals the strong non-linearity of electrolyser at lower current density.

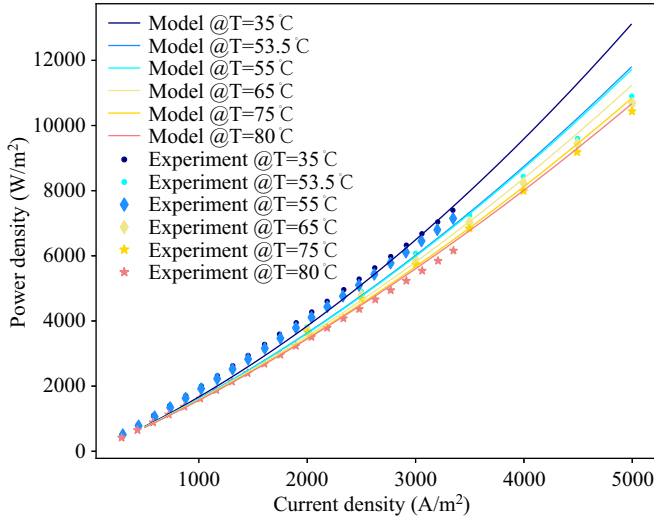


Fig. 3. The comparison of simulation and experimental results. The real experiment data are obtained from [30] 55°C, 65°C, 75°C, and from [31] at 35°C, 53.5°C, 80°C.

process is adiabatic, the power consumption p_{comp} (W) at a certain mass flow rate \dot{m}_{H_2} (kg/s) is represented as:

$$p_{\text{comp}} = \frac{RT_{\text{in}}}{2(\gamma - 1)\eta_c} \left(\left(\frac{P_{\text{out}}}{P_{\text{in}}} \right)^{\frac{\gamma-1}{\gamma}} - 1 \right) \dot{m}_{\text{H}_2} \quad (15)$$

where T_{in} is the inlet temperature of compressor (K), P_{in} and P_{out} represent the inlet and outlet pressure (Pa), γ is the isotropic exponent, η_c is the efficiency of mechanical compressor, generally between 0.4 and 0.75 [32].

D. Hydrogen Tank

In the studied system, without loss of generality, it is assumed that hydrogen is firstly compressed and stored in the tank and then consumed or transported. Compressed gaseous hydrogen storage is the most common technique [33]. To calculate the amount of hydrogen that is stored in a hydrogen tank, we use the following equation:

$$M_{\text{H}_2,t} = M_0 + \int_0^t (\dot{n}_{\text{H}_2,\text{in}} - \dot{n}_{\text{H}_2,\text{out}}) dt \quad (16)$$

where $M_{\text{H}_2,t}$ is the amount of hydrogen in the tank at time t (mol), and M_0 the initial amount (mol). $\dot{n}_{\text{H}_2,\text{in}}$ is the inlet molar flow rate (mol/s) and $\dot{n}_{\text{H}_2,\text{out}}$ outlet molar flow (mol/s).

III. TWO-STAGE MULTI-OBJECTIVE OPTIMIZATION ON DESIGN AND OPERATION

A two-stage optimization method is established to reveal the interaction between system planning and operation strategies. System planning refers to a long-term decision of sizing the components before implementation. System planning/design/investment are all analogous studies emphasizing on the problem resolution for optimal sizing/configuration at the phase of planning/design/investment. System operation strategies, on the other hand, form the short-term decisions that deal with the dispatch and scheduling of one or more components. The operation strategies could vary according to different objectives. Both planning and operation are coupled in this two-stage optimization scheme.

Figure 4 illustrates the framework of the two-stage optimization. The inner loop aims at providing the system with optimal operational strategies where different objectives (economic benefits maximization, green hydrogen maximization, etc.) could be employed. The outer loop deals with the balance of long-term system financial profits and inner operational objectives. The primary variables in this layer are mainly the sizes of the involved components. Given a specific operational strategy, the multi-objective optimization algorithm in the outer layer tends to find the Pareto optimal solutions for system planning.

The inner and outer optimization in this scheme is decoupled, facilitating the execution of planning according to diverse operational strategies. Previous studies on planning used to consider one or more selected operation strategies. In the contemporary energy system, wherein regulations, markets, and latest services change rapidly, the goal of operation is also bound to change to adapt to the new environment. This necessitates the consideration of different operation strategies into planning.

A. Outer Layer Optimization

The outer layer considers the trade-off between long-term economic benefits and short-term operational objectives. For a typical HWHS, five principal components are taken into account in this study: wind turbine, electrolyser, compressor, converter and hydrogen tank. To simplify this optimization problem, while maintaining the foremost planning choice, the following assumptions are made: 1) It is assumed that the capacities of the converter and the compressor are both linearly proportional to the electrolyser capacity. 2) Among the remaining three variables, the capacity of the wind turbine is set to be fixed, which could be viewed as a metrics of system scale. It could be influenced by the wind resources, electricity and hydrogen loads, as well as by the capacity of transmission lines. This assumption signifies that the wind turbines have been already installed and accordingly, the corresponding

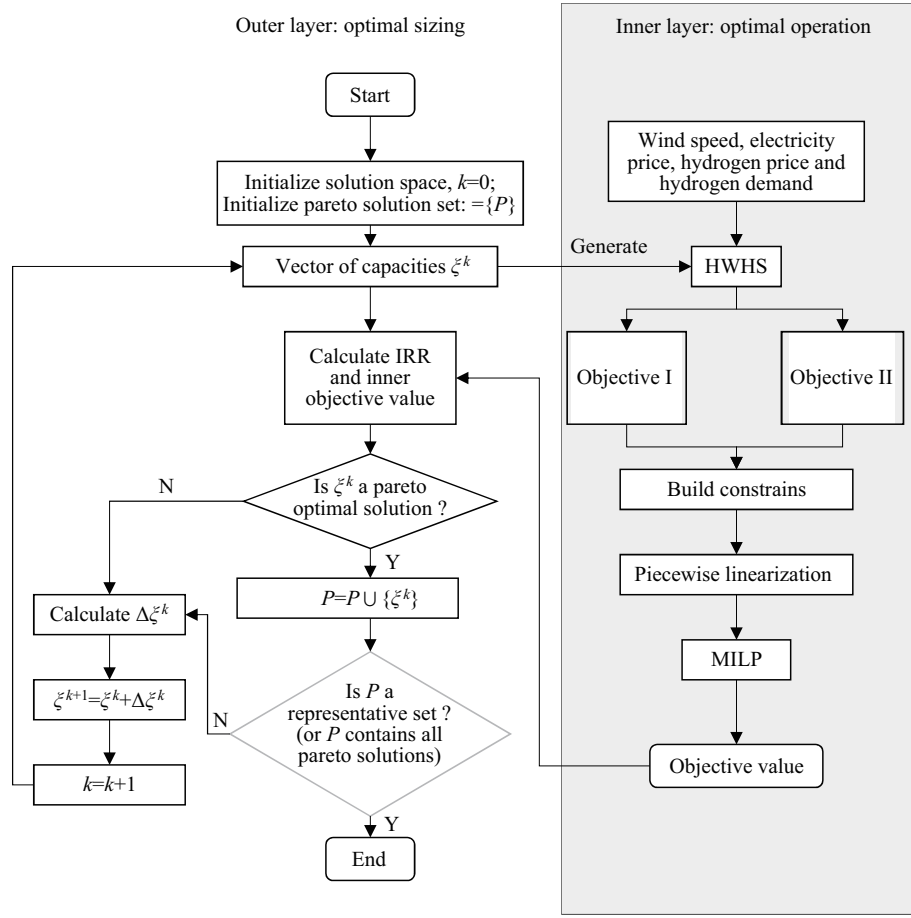


Fig. 4. Two-layer multi-objective optimization: the inner loop focuses on system operational strategies using mixed integer linear programming; the outer loop solves the multi-objective problem concerning system planning and optimal operation.

electrolyzers and hydrogen storage can be planned. In fact, for a system planning with three variables, e.g., a, b, c , it is always feasible to only consider b/a and c/a , and let a be a predetermined parameter. 3) The total electricity and hydrogen loads are pre-specified in accordance with wind turbine capacity. Therefore, the outer layer multi-objective optimization could be formulated as:

$$\begin{aligned} & \max_{C_e, C_t} \{ \text{IRR}, \text{OF} \} \\ & \text{s.t. } C_{e,\min} \leq C_e \leq C_{e,\max} \\ & \quad C_{t,\min} \leq C_t \leq C_{t,\max} \end{aligned} \quad (17)$$

where C_e and C_t are the capacities of electrolyser and hydrogen, respectively (MW and kg), and the upper and lower bounds rely on the specific conditions in different projects, such as available space, investment budgets and security requirements. IRR is the internal rate of return for a specific project. OF is the operational objective function. The planners prefer to maximize IRR by choosing appropriate capacity combinations, whereas oversizing could yield additional flexibility, which generally contributes to short-term operational benefits. The planners are required to make a trade-off. For example, a larger hydrogen tank may enable higher green hydrogen production, but would also require a higher initial investment.

IRR is defined as the discount rate i_r that makes the system

net present value (NPV) zero.

$$\text{NPV}(i_r = \text{IRR}) = 0 \quad (18)$$

where NPV is widely used in capital budgeting and investment planning to estimate system profitability. By considering all the revenue flows for the future, NPV represents the difference between the present value of cash inflows and outflows over the project lifespan. Increased NPV will result in larger IRR; if NPV is negative, so would be IRR. To calculate NPV, a presupposed discount rate is necessary, but it is not possible to get an accurate forecast of the discount rate in the lifespan of this project. Meanwhile, since this paper aims at giving a generic understanding of HWHS, the absolute value of profits are unnecessary, and thus IRR is employed. The relationship between NPV and i_r is formulated as:

$$\text{NPV} = \sum_{L=1}^{L_{\text{pro}}} \frac{\text{Prof}_i}{(1 + i_r)^L} - \text{NPC} \quad (19)$$

where Prof_i is the expected income cash flow for the i th year (€); NPC is the net present value of costs (€); L_{pro} is the lifespan of the project (year). Prof_i is described as:

$$\text{Prof}_i = \sum_{t=1}^{8760} ((p_{u,t} + p_{l,t})\bar{\pi}_t + \bar{m}_{l,H_2,t}\bar{\pi}_{H_2,t})\Delta t \quad (20)$$

Here, the $\bar{\pi}_t$ and $\bar{\pi}_{H_2,t}$ are the price of electricity (€/MWh) and hydrogen respectively (€/kg), and Δt , the time resolution, is one hour. $\bar{\pi}_t$ varies with time whereas $\bar{\pi}_{H_2,t}$ is presumed to remain unchanged. The $p_{u,t}$ and $p_{l,t}$ are the electricity sold to utility grid and to internal consumers (MW). $\bar{m}_{L,H_2,t}$ is the hydrogen consumption at time t (kg/h). NPC is calculated by:

$$NPC = C_{cap} + C_{O\&M} + C_{rep} - C_{salv} \quad (21)$$

with C_{cap} denoting the present value of capital cost (€), $C_{O\&M}$ indicating the present value of operation and maintenance cost (€), C_{rep} being the present value of replacement cost (€), C_{salv} denoting the residual value or salvage value of components (€), which is disregarded in this study. The capital cost is calculated as:

$$C_{cap} = \sum_i C_i C_{cap,i}, i = wt, ele, tank, conv, comp \quad (22)$$

where C_i and $C_{cap,i}$ are the capacity and capital cost for component i . The operation and maintenance cost is:

$$C_{O\&M} = \sum_i \sum_{L=1}^{L_{pro}} C_{O\&M,i} \frac{1}{(1+i_r)^L} \quad (23)$$

The replacement cost depends on the lifespan of different components:

$$C_{rep} = \begin{cases} \sum_i \sum_{Y=1}^{Y_{rep}} C_{rep,i} \cdot \frac{1}{(1+i_r)^{L_{rep,i}Y}}, & Y_{rep} > 0 \\ 0, & Y_{rep} = 0 \end{cases} \quad (24)$$

where $L_{rep,i}$ is the life span of component i and $Y_{rep,i}$ is the count of replacing component i , expressed as:

$$Y_{rep} = \left\lfloor \frac{L_{pro}}{L_{rep,i}} \right\rfloor - 1 \quad (25)$$

TABLE I
ECONOMIC PARAMETERS FOR INVOLVED COMPONENTS

Component	Unit	Capital cost (€/unit)	Annual O&M cost (€/unit)	Life span (year)
Wind turbine	kW	1547	56	20
Electrolyser	kW	1492	60	20
Hydrogen tank	kg	854	8	20
Compressor	kg/h H2	13338	666	20
Converter	kW	126	-	15

The other objective function OF for out-loop is the operational objective that is defined in the inner loop, which represents the operators' strategies.

To solve this multi-objective optimization problem, NSGAI (non-dominated sorting genetic algorithm) is utilized [34]. By introducing non-dominated sorting and crowd distance sorting, it is effective to solve multi-objective problems [35]. The flow diagram is shown in Fig. 5, briefly describing the process.

B. Inner Layer Optimization

1) Environmental Parameters

The wind power, electricity price, power load and hydrogen load profiles are the most important parameters that should be taken into account. These parameters are typically viewed as uncertain ones that can be depicted using stochastic estimation and Monte Carlo method [36], [37]. As handling the involved

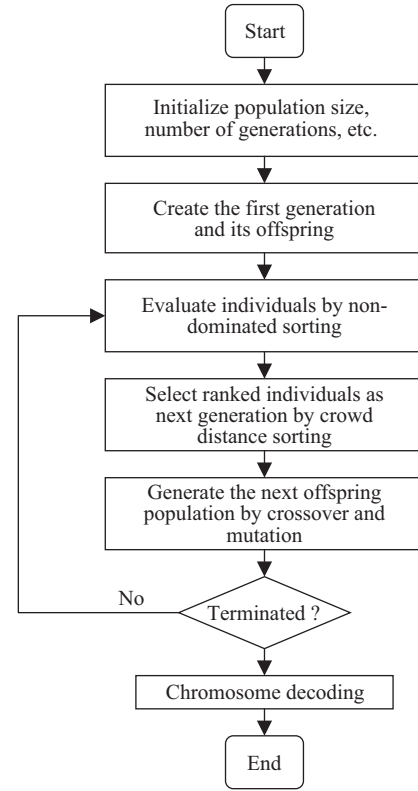


Fig. 5. Flowchart of NSGAI algorithm. This method inherits the basic ideas of mutation and crossover in genetic algorithm. By introducing non-dominated sorting and crowd distance sorting, it is well designed to cope with multi-objective optimization problem.

uncertainties is not the primary purpose of this paper, historical real data of wind speed etc., are simply used to conduct the inner layer optimization. By considering the yearly environmental data, mixed-integer linear programming is introduced to optimize the operation.

2) Inner Objective Function

The inner loop objectives are subjective to the choice of the system operator. It can generally be opted to maximize multiple profits in the system, or can also be used to produce additional green hydrogen that is beneficial to sustainability.

$$OF^I = \max \sum_{t=1}^T \{p_{u,t} \bar{\pi}_t \Delta t + \dot{m}_{H_2,t} \bar{\pi}_{H_2,t} \Delta t - p_{ele,t} C_{m,ele} \Delta t - p_{comp,t} C_{m,comp} \Delta t\} \quad (26)$$

As shown in (26), the objective function OF^I is expected to maximize the system operational profits. The definitions of $p_{u,t}$, $\bar{\pi}_t$, $\bar{\pi}_{H_2,t}$ remain the same with the ones in NPV calculation. Hydrogen price is assumed to be around 5€/kg in this paper. $p_{ele,t}$ is the electrolyser power (MW) and $C_{m,ele}$ is the cost of water that is needed to produce hydrogen (€/MWh). $p_{comp,t}$ represents the power of compressor (MW) and $C_{m,comp}$ is the corresponding fuel cost (€/MWh).

$$OF^{II} = \frac{\sum_{t=1}^T \dot{m}_{H_2,t,g}}{\sum_{t=1}^T \bar{m}_{L,H_2,t}} \quad (27)$$

Objective function OF^{II} is expected to maximize the green hydrogen proportion of hydrogen consumption. $\dot{m}_{H_2,t,g}$ is

the green gas production (kg/h), referring to those generated totally by renewable energy. $\bar{m}_{L,H_2,t}$ is the total hydrogen consumption at time t (kg/h).

3) Constraints for Objective Function I

Equation (28) describes the energy conservation of the whole system. Note that the transmission loss has been neglected due to short distances.

$$\bar{p}_{w,t} - p_{u,t} - \bar{p}_{L,t} - p_{\text{comp},t} - p_{\text{ele},t} = 0, \quad \forall t > 0 \quad (28)$$

where $\bar{p}_{w,t}$ and $\bar{p}_{L,t}$ are wind power and electric loads respectively (MW). The change of hydrogen in the tank is depicted as follows:

$$M_t^{\text{Ht}} - M_{t-1}^{\text{Ht}} = \dot{m}_{H_2,t} \Delta t - \bar{m}_{L,H_2,t} \Delta t, \quad \forall t \geq 1 \quad (29)$$

with $\dot{m}_{H_2,t}$ denoting the hydrogen production rate (kg/h). As illustrated in section two, the relation between \dot{m}_{H_2} and p_{ele} is slightly non-linear, which is linearized in the following section. We have:

$$\dot{m}_{H_2,t} = \dot{m}_{H_2,t}(p_{\text{ele},t}) \quad (30)$$

The initial hydrogen in the tank is defined as M_{ini} , that is:

$$M_0^{\text{Ht}} = M_{\text{ini}} = M_T^{\text{Ht}} \quad (31)$$

Meanwhile, the mass of hydrogen M_t^{Ht} (kg) that can be stored is limited by the SoC (State of Charge) limits of the tank:

$$C_t \underline{\text{SoC}} \leq M_t^{\text{Ht}} \leq C_t \overline{\text{SoC}} \quad (32)$$

It is also assumed that the initial and final hydrogen levels should remain the same to assure a continuous operation. Concerning the electrolyser, there are several technical constraints. The lower bound of electrolyser power could be nearly zero for PEM or SOEC. However, as far as AEL is concerned, this bound is important to its safety operation because, at low current density, the generated hydrogen and oxygen could form a potentially flammable mixture by gas diffusion [38], [39]. Thus, commercially available AEL generally works above 20% of its nominal current density, as shown in (33). The power change of electrolyser is limited to its ramping rate, as presented in (34) and (35), where the RLU represents ramping rate limit upward and RLD is the downward limit. Both are rather fast. For example, as indicated in [17], an AEL could change its power by $\pm 20\%$ of its nominal power per second. Therefore, this constraint is in fact negligible in terms of an hourly operation.

$$0.2C_e \leq p_{\text{ele},t} \leq C_e, \quad \forall t > 0 \quad (33)$$

$$p_{\text{ele},t+1} - p_{\text{ele},t} \leq \text{RLU} \quad \forall t > 0 \quad (34)$$

$$p_{\text{ele},t+1} - p_{\text{ele},t} \geq -\text{RLD} \quad \forall t > 0 \quad (35)$$

With regard to the compressor, (15) indicates the power consumed is proportional to hydrogen mass flow rate when the inlet temperature, pressure and outlet pressure are pre-designed. This is simply summarized as (37):

$$p_{\text{comp}} \leq p_{\text{comp},t} \leq \bar{p}_{\text{comp}}, \quad \forall t > 0 \quad (36)$$

$$p_{\text{comp},t} = \alpha_c \dot{m}_{H_2,t}, \quad \forall t > 0 \quad (37)$$

with α_c as a constant dependent on working parameters.

4) Constraints for Objective Function II

The green hydrogen and electrolysis should be defined when considering objective function II. All the constraints listed in the previous section still apply to this new problem and apart from these, new constraints regarding green production are added.

$$\dot{m}_{H_2,t,g} = \dot{m}_{H_2,t,g}(p_{\text{ele},t,g}), \quad \forall t > 0 \quad (38)$$

Green hydrogen is produced from renewable energy, whose production rate, $\dot{m}_{H_2,t,g}$, is also a non-linear function of electrolyser power. $p_{\text{ele},t,g}$ should satisfy the following equations:

$$p_{\text{ele},t,g} \leq \bar{p}_{w,t}, \quad \forall t > 0 \quad (39)$$

$$p_{\text{ele},t,g} \leq p_{\text{ele},t}, \quad \forall t > 0 \quad (40)$$

where $p_{\text{ele},t,g}$ is an imaginary variable that shows a measure of the extent to which the energy used by the electrolyser is green. These two equations are natural description in light of its definition.

5) Piece-wise Linearization

As shown in Fig. 2, to better simulate the electrolyser properties, a non-linear model is needed. We introduce a few integer variables to linearly express the functions in (30) and (38). A piece-wise linear function with three pieces is used to approximate the original production curve and correspondingly, two breakpoints are introduced as $b_{\text{ele},1}$, $b_{\text{ele},2}$. The boundary points are denoted as $b_{\text{ele},0}$ and $b_{\text{ele},3}$, therefore, $\dot{m}_{H_2,t}$ can be formulated as:

$$\dot{m}_{H_2,t} = \sum_{i=0}^3 w_i \dot{m}_{H_2,t}(b_{\text{ele},i}) \quad (41)$$

with w_i representing the weight and it should satisfy:

$$\sum_{i=0}^3 w_i = 1, w_i \geq 0 \quad (42)$$

It should also meet the following requirements:

$$\begin{aligned} w_0 &\leq z_1 \\ w_1 &\leq z_1 + z_2 \\ w_2 &\leq z_2 + z_3 \\ w_3 &\leq z_3 \end{aligned} \quad (43)$$

where z_i is a binary variable and it fulfills:

$$\sum_{i=1}^3 z_i = 1 \quad (44)$$

The above equations ensure that at most two adjacent w_i could be nonzero. More details are available in [40].

IV. CASE STUDY: AN ON-GRID WIND HYDROGEN HYBRID SYSTEM IN DENMARK

Denmark has been incessantly focusing on renewable green energy. GreenLab Skive (GLS) is a green energy industrial park located in western Denmark (see Fig. 6). Thirteen wind turbines and solar panels are currently being developed in this area along with several chemical plants that serve as hydrogen off-takers. GLS offers a remarkable opportunity for the

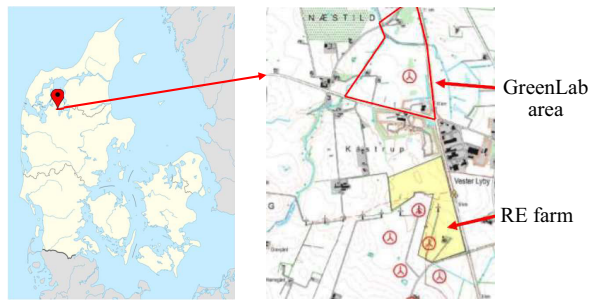


Fig. 6. Location of GreenLab Skive, Latitude: 56.64 Longitude: 8.97.

analysis and trial of innovative technologies. It incorporates a complete electrolysis system that serves as the main hydrogen supplier for the involved stakeholders. The hydrogen is first produced by an alkaline electrolyser and then compressed to 200 bar, stored in a tank and sold to the users. We examine the proposed method to evaluate the economics and sustainability of this HWHS.

Figure 7 shows the annual environmental historical data. The wind speed data can be found on the website [41] and the price data come from Nordpool spot market [42]. As the involved consumers in this area are mostly chemical plants, both the power loads and hydrogen loads tend to be stable. Most consumers have their own production schedule and continuous operation plans. The load profile can be found in Fig. 8. In this study, the inner layer optimization is firstly calculated based on these input parameters over a year and

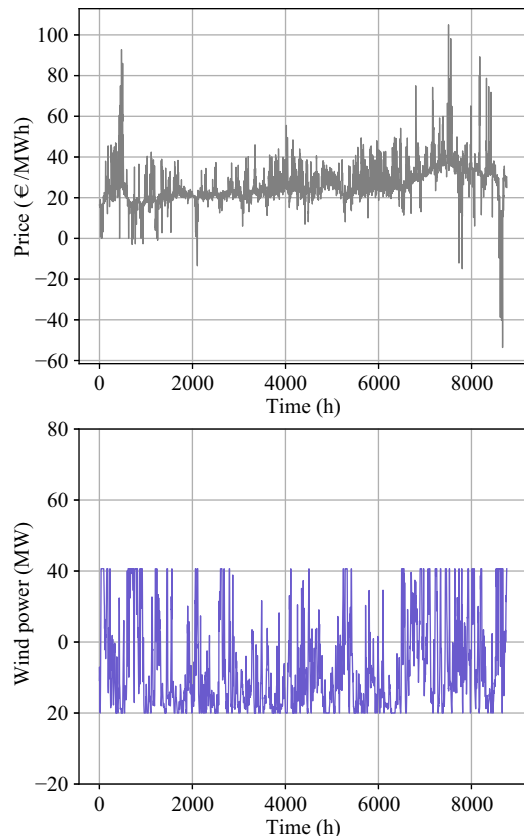


Fig. 7. Electricity price and wind power over a year.

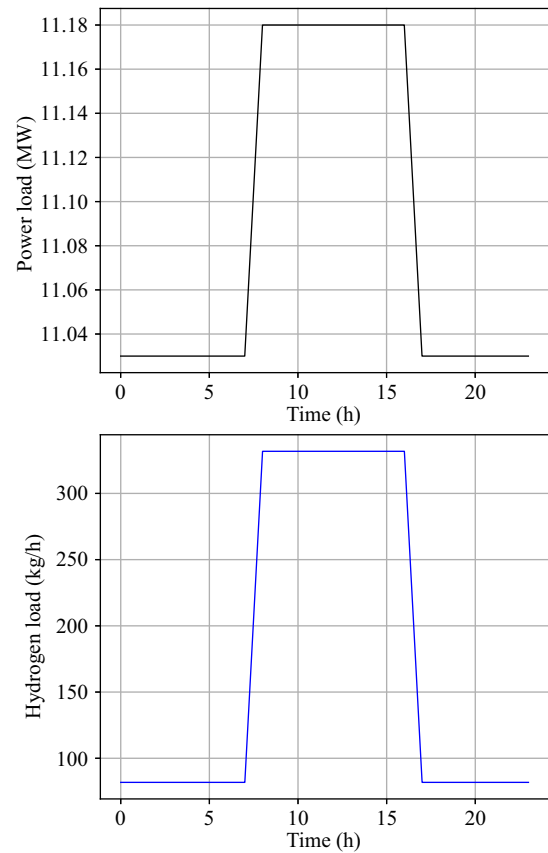


Fig. 8. Power and hydrogen loads in a day. It is assumed that over a year, the daily load profile is identical since the consumption levels are stable.

then the outer loop is employed to find a trade-off between operational goals and planning objectives. Using prediction data or scenario-based stochastic optimization in the inner layer is more realistic. But to keep the optimization framework simple, the historical data are utilized.

V. RESULTS AND DISCUSSION

A. Inner Layer Optimization Results

The inner loop is expected to optimize system operation based on different objectives. Since the electrolyser is the key component in this system, the main issue is determining its dispatch curve. In the case of maximizing economic profits, the dispatch curve of the electrolyser is illustrated in Fig. 9. To clearly show the results, a three-day calculation is conducted, instead of a whole year. It is observed that to obtain more revenues in the power spot market, the electrolyser power is significantly affected by the price signals. When the electricity price is high (e.g. from hour 10 to 20, 40 to 45 and 60 to 70), the electrolyser tends to consume less electricity. This tendency does not get affected by wind energy because with abundant wind energy, the decrease in electrolyser power enables the system to sell electricity, while with insufficient wind energy, the power reduction helps to avoid using expensive electricity to produce hydrogen. Likewise, for the lower electricity price (from hour 0 to 10, 20 to 30), the electrolyser tends to reach its maximal production. The correlation coefficient between price and electrolyser power is

sizes, has a larger gradient when the sizes are relatively small. It is also revealed that when the tank size is extremely small, the electrolyzer capacity generates only minimal influence on the inner objective; as the tank size increases, its influence becomes larger. Overall, the entire trend implies that the profit is more susceptible to hydrogen storage. It is also observed that the marginal utility induced by increased size declines as the size gets larger. That is, to obtain the same amount of profits, more investment on hydrogen storage and electrolyser becomes essential. The absolute increase of the optimal profit is small, which suggests that the ability to improve operational profits is not so sensitive to these two factors provided that the system only participates in the spot market.

The sensitivity analysis for inner objective II is depicted in Fig. 13. It reveals that the maximal green hydrogen proportion can be acquired when the tank size is large, whereas this objective is far less sensitive to electrolyser capacity. When the hydrogen storage is sufficiently large, electrolyser capacity starts to significantly affect the green hydrogen proportion. A larger electrolyser enables the system to produce more hydrogen when renewable energy is abundant, but as shown in Fig. 11, the tank SoC imposes a stronger constraint on this system. If the tank size is small, even though a large electrolyser is installed, the amount of green hydrogen is still limited. In the studied system, all the hydrogen is firstly stored in the tank and then consumed, and is not utilized directly.

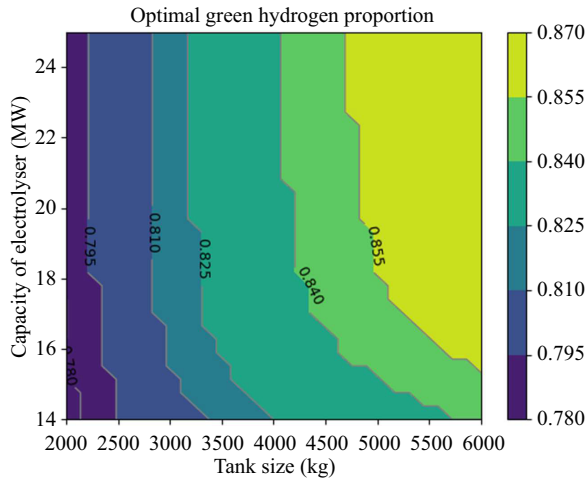


Fig. 13. Influence of system sizing on maximal green hydrogen proportion for over a year.

C. Outer-layer Optimization Results

As suggested in sensitivity analysis, system planning has a great influence on system operational objectives, and there is a trade-off between initial investment and operational flexibility. For instance, larger hydrogen storage, on the one hand, improves the ability to obtain revenues; on the other hand, it demands huge initial investment, thereby decreasing IRR. Taking the inner objective I and IRR as two objectives, Fig. 14 illustrates the result of this multi-objective problem. From point A to B, the IRR decreases dramatically, whereas the optimal annual profits rise slowly, and from point B to C and D, the IRR almost remains the same, while there is a

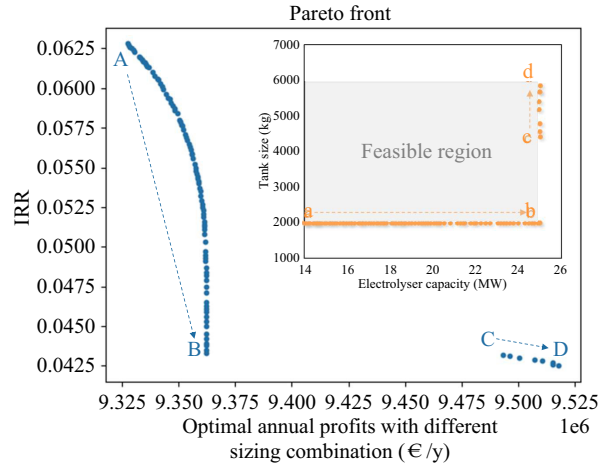


Fig. 14. Pareto front of the multi-objective optimization coping with the trade-off between system investment payback (IRR) and optimal operational profits.

relatively large increase in annual profits. The sub-figure gives the corresponding combinations of electrolyser capacity and tank size. The results indicate that albeit larger sizing allows the system to derive more benefits from the spot market, it is not economical due to large initial investment. In reality, the system should be planned at point A, sacrificing the flexibility to reduce the initial investment. Interestingly, all the Pareto optimal solutions fall under the boundary of the feasible region. By simplifying this multi-objective problem, a mathematical proof on the necessity is given in appendix A.

Figure 15 displays the result of outer-loop with respect to inner objective II—optimal green hydrogen proportion. Fewer Pareto optimal solutions are found in this case. It is observed that to make the system capable of producing more green hydrogen, more investments are needed, even though they reduce the IRR. Point A is the one with the highest IRR, and correspondingly, the tank size is 2000 kg and electrolyser capacity is 17 MW. From point B to C, the capacity of the electrolyser remains the same but the tank size gradually increases. The result implies that the system planner must consider the trade-off between green hydrogen production and

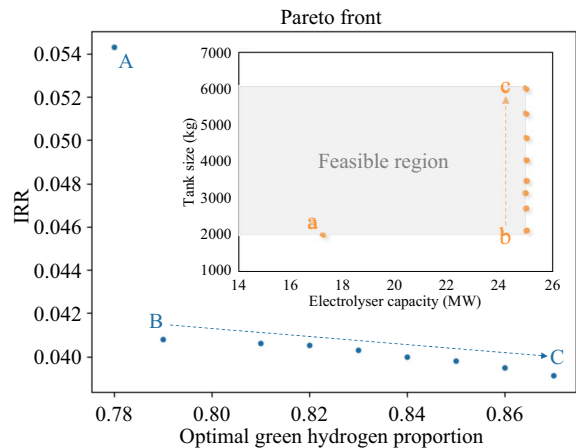


Fig. 15. The trade-off between high IRR and additional green hydrogen production, shown as a Pareto front.

the initial investment. To obtain maximal green hydrogen, the system should be designed at point C. It is also noteworthy that the largest IRR (5.5%) in this case is less than the one for the previous result (6.25%), which reflects the different emphasis of the two operational strategies.

There are two important factors that need to be highlighted. Concerning the first multi-objective problem, the system gains more flexibility at a cost of low IRR. However, this flexibility is only utilized in the spot power market, limiting the scope of its potential value. It is valuable to shed light upon how the flexibility could be further priced and used. If, for instance, the electrolyser can be utilized to provide services in the balancing market (which is feasible because an electrolyser has a fast response speed), more revenues could be generated. Utilizing AEL to improve power system frequency stability is also a potential option to employ its flexibility. Considering these possibilities, a more complex relationship between IRR and system operational flexibility can be obtained. Another issue is in the green hydrogen premium, which could intensify the competitiveness for green hydrogen. On the condition that the price of green hydrogen is larger than its ordinary counterpart, the IRR and green hydrogen proportion may not be strongly negatively correlated. New trade-offs will be found under this assumption. However, these problems are beyond this paper and demand more comprehensive studies and solutions in the future.

VI. CONCLUSION

In this study, a two-layer hybrid optimization algorithm is presented to analyze the trade-off between system operation and planning for a typical HWHS. This optimization is firstly carried out with respect to the system operation and then applied to system planning. Two operational objectives are taken into account.

It was found that based on an operational purpose, the dispatch of the electrolyser exhibits different tendencies. The electrolyser considerably responds to price signals when the operational objective is to maximize the profits, whereas it is more susceptible to the amount of green renewable energy in the case of producing more green hydrogen. The system operational flexibility depends on its design. The sensitivity analysis on the influence of sizing reveals that both the increase of the electrolyser installed capacity and hydrogen storage size result in enhanced system performance irrespective of the chosen objective. It is actually the flexibility conferred by the design that enables the system to operate in a better way. Nevertheless, this flexibility comes at the cost of a larger initial investment. It is reasonable to conclude, to some extent, that the trade-off between system operation and planning is the one between initial investment and potential flexibility.

The outer-layer multi-objective optimization based on NS-GAII clearly illustrates this balance. However, the result concerning operational objective of economics suggests that the additional flexibility is uneconomical and the system should be sized to get the highest IRR (i.e., 14 MW electrolyser and 2000kg hydrogen storage in this paper). This conclusion is limited to the fact that the added flexibility is only used

for energy arbitrage in the spot market. The optimized results on the trade-off between IRR and green hydrogen production reflect the same trend. To gain an increase of 10% in green hydrogen proportion, the IRR decreases by 1.2%. Whether this is beneficial relies on the choice of stakeholders. For example, to gain the maximum green hydrogen, the electrolyser and hydrogen storage should be about 25 MW and 6,000 kg, respectively, although the IRR is relatively small. It is also essential to note that no green hydrogen premium is considered, which could further affect the conclusions.

Forthcoming research will emphasize on the pricing of the added flexibility and sustainability, as well as the inclusion of other planning and operation objectives in order to achieve a more comprehensive understanding of the trade-off between strategies and objectives deployed at operation and planning phases. Employing forecast and stochastic optimization to further analyze this problem in broad terms will be an advancement of this work.

VII. ACKNOWLEDGEMENT

The authors would like to acknowledge financial support from ‘‘Synergies Utilising renewable Power Regionally by means of Power to Gas project’’, which received funding in the framework of the joint programming initiative ERA-Net Smart Energy Systems’ focus initiative Integrated, Regional Energy Systems, in collaboration with support from the European Union’s Horizon 2020 research and innovation program under grant agreement No. 775970.

APPENDIX

As shown in Fig. 14, all the Pareto solutions fall along the boundary of the feasible region. In this section, a brief proof is given by simplifying the objective function. Let:

$$E \in [C_{e,\min}, C_{e,\max}] \quad (45)$$

$$T \in [C_{t,\min}, C_{t,\max}] \quad (46)$$

$$F = E \times T = \{(e, t) | e \in E, t \in T\} \subset \mathbb{R}^2 \quad (47)$$

F is the feasible region of the optimization problem, which is a subset of \mathbb{R}^2 . The objective is to demonstrate that all Pareto solutions, in the form of $(f_1, f_2) \in F$, are located on the boundary of F . We assume in the following a logistic shape of the out-layer and inner-layer objective function:

$$\begin{cases} Obj_1(\vec{f}) = -c_1 f_1 - c_2 f_2 + c_3 Obj_2(\vec{f}), c_i > 0 \\ Obj_2(\vec{f}) = A \left(1 - e^{-\frac{\alpha_1 f_1 - \alpha_2 f_2}{\beta}} \right), \alpha_1, \alpha_2, \beta > 0 \end{cases} \quad (48)$$

$Obj_1(\vec{f})$ briefly describes the relation between system NPV and f_1, f_2 . Since maximizing IRR is identical with finding maximal NPV, the optimal solutions of $Obj_1(\vec{f})$ are the same as those for the primal problem. $Obj_2(\vec{f})$ is an estimate of inner objective function based on the sensitivity analysis. It does not have to be applicable for the entire F . As long as the inner objective function could be approximated by a function in the form of $Obj_2(\vec{f})$ in an infinitesimal closed set of F , the following demonstration will make sense.

Given an infinitesimal increment of f , $d\vec{f} = (df_1, df_2)$, we have:

$$\Delta Obj_1(\vec{f}) = -c_1 df_1 - c_2 df_2 + \Delta Obj_2(f) \quad (49)$$

$$\begin{aligned} \Delta Obj_2(\vec{f}) &= -Ae^{\frac{-\alpha_1 f_1 - \alpha_2 f_2}{\beta}} \left(-\frac{\alpha_1 df_1}{\beta} - \frac{\alpha_2 df_2}{\beta} \right) \\ &= \frac{A}{\beta} e^{\frac{-\alpha_1 f_1 - \alpha_2 f_2}{\beta}} (\alpha_1 df_1 + \alpha_2 df_2) \end{aligned} \quad (50)$$

The method of proof by contradiction has been used to show there is no such \vec{f}^* satisfying $\vec{f}^* \notin \partial F$ and \vec{f}^* is a Pareto optimal solution ($f^* \in P_F$) of this problem. Assuming $\exists \vec{f}^* = (f_1^*, f_2^*) \in P_F$ and $(f_1^*, f_2^*) \notin \partial F$, we have:

If

$$\frac{\alpha_2}{\alpha_1} > \frac{c_2}{c_1} \quad (51)$$

Then:

$$\exists df_2^* > 0 \quad \text{and} \quad df_1^* = -\frac{c_2}{c_1} df_2^* < 0 \quad (52)$$

Such that:

$$\vec{f}_1^* = (f_1^* + df_1^*, f_2^* + df_2^*) \in F \quad (53)$$

$$\Delta Obj_2 = \frac{A}{\beta} e^{\frac{-\alpha_1 f_1^* - \alpha_2 f_2^*}{\beta}} \left(\alpha_2 - \frac{\alpha_1 c_2}{c_1} \right) df_2^* > 0 \quad (54)$$

$$\Delta Obj_1 = c_3 \Delta Obj_2 > 0 \quad (55)$$

Thus, we found $\vec{f}_1^* \in F$ and $Obj_1(\vec{f}_1^*) > Obj_1(\vec{f}^*)$, $Obj_2(\vec{f}_1^*) > Obj_2(\vec{f}^*)$. This contradicts the assumption that $\vec{f}^* = (f_1^*, f_2^*) \in P_F$ because we found another $\vec{f}_1^* \in F$ that dominates \vec{f}^* .

If

$$\frac{\alpha_2}{\alpha_1} < \frac{c_2}{c_1} \quad (56)$$

Then:

$$\exists df_1^* > 0 \quad \text{and} \quad df_2^* = -\frac{c_1}{c_2} df_1^* < 0 \quad (57)$$

Such that:

$$\vec{f}_1^* = (f_1^* + df_1^*, f_2^* + df_2^*) \in F \quad (58)$$

$$\Delta Obj_2 = \frac{A}{\beta} e^{\frac{-\alpha_1 f_1^* - \alpha_2 f_2^*}{\beta}} \left(\alpha_1 - \frac{\alpha_2 c_1}{c_2} \right) df_1^* > 0 \quad (59)$$

$$\Delta Obj_1 = c_3 \Delta Obj_2 > 0 \quad (60)$$

Again, \vec{f}_1^* dominates \vec{f}^* , which contradicts the assumption.

REFERENCES

- [1] H. Ishaq and I. Dincer, "Evaluation of a wind energy based system for co-generation of hydrogen and methanol production," *International Journal of Hydrogen Energy*, vol. 45, no. 32, pp. 15869–15877, Jun. 2020, doi: 10.1016/j.ijhydene.2020.01.037.
- [2] S. Bourne, "The future of fuel: The future of hydrogen," *Fuel Cells Bulletin*, vol. 2012, no. 1, pp. 12–15, Jan. 2012.
- [3] M. Bailera, P. Lisbona, L. M. Romeo, and S. Espatolero, "Power to Gas projects review: Lab, pilot and demo plants for storing renewable energy and CO₂," *Renewable and Sustainable Energy Reviews*, vol. 69, pp. 292–312, Mar. 2017, doi: 10.1016/j.rser.2016.11.130.
- [4] M. Thema, F. Bauer, and M. Sterner, "Power-to-Gas: Electrolysis and methanation status review," *Renewable and Sustainable Energy Reviews*, vol. 112, pp. 775–787, Sep. 2019, doi: 10.1016/j.rser.2019.06.030.
- [5] O. M. Balan, M. R. Buga, A. Brunot, A. Badea, and D. Froelich, "Technical and economic evaluation of Power-to-Gas in link with a 50 MW wind park," *Journal of Energy Storage*, vol. 8, pp. 111–118, Nov. 2016, doi: 10.1016/j.est.2016.10.002.
- [6] I. Firtina-Ertis, C. Acar, and E. Erturk, "Optimal sizing design of an isolated stand-alone hybrid wind-hydrogen system for a zero-energy house," *Applied Energy*, vol. 274, pp. 115244, Sep. 2020.
- [7] S. M. Muyeen, R. Takahashi, and J. Tamura, "Electrolyzer switching strategy for hydrogen generation from variable speed wind generator," *Electric Power Systems Research*, vol. 81, no. 5, pp. 1171–1179, May 2011.
- [8] S. Rahimi, M. Meratizaman, S. Monadizadeh, and M. Amidpour, "Techno-economic analysis of wind turbine-PEM (polymer electrolyte membrane) fuel cell hybrid system in standalone area," *Energy*, vol. 67, pp. 381–396, Apr. 2014, doi: 10.1016/j.energy.2014.01.072.
- [9] C. Jørgensen and S. Ropenus, "Production price of hydrogen from grid connected electrolysis in a power market with high wind penetration," *International Journal of Hydrogen Energy*, vol. 33, no. 20, pp. 5335–5344, Oct. 2008.
- [10] O. J. Guerra, J. Eichman, J. Kurtz, and B. M. Hodge, "Cost competitiveness of electrolytic hydrogen," *Joule*, vol. 3, no. 10, pp. 2425–2443, Oct. 2019.
- [11] F. Griiger, O. Hoch, J. Hartmann, M. Robinus, and D. Stolten, "Optimized electrolyzer operation: Employing forecasts of wind energy availability, hydrogen demand, and electricity prices," *International Journal of Hydrogen Energy*, vol. 44, no. 9, pp. 4387–4397, Feb. 2019.
- [12] A. Maleki, H. Hafeznia, M. A. Rosen, and F. Pourfayaz, "Optimization of a grid-connected hybrid solar-wind-hydrogen CHP system for residential applications by efficient metaheuristic approaches," *Applied Thermal Engineering*, vol. 123, pp. 1263–1277, Aug. 2017.
- [13] J. G. G. Clua, R. J. Mantz, and H. De Battista, "Optimal sizing of a grid-assisted wind-hydrogen system," *Energy Conversion and Management*, vol. 166, pp. 402–408, Jun. 2018.
- [14] Z. H. Deng and Y. W. Jiang, "Optimal sizing of wind-hydrogen system considering hydrogen demand and trading modes," *International Journal of Hydrogen Energy*, vol. 45, no. 20, pp. 11527–11537, Apr. 2020.
- [15] G. M. Yang, Y. W. Jiang, and S. You, "Planning and operation of a hydrogen supply chain network based on the off-grid wind-hydrogen coupling system," *International Journal of Hydrogen Energy*, vol. 45, no. 41, pp. 20721–20739, Aug. 2020, doi: 10.1016/j.ijhydene.2020.05.207.
- [16] A. Dolatabadi, R. Ebadi, and B. Mohammadi-Ivatloo, "A two-stage stochastic programming model for the optimal sizing of hybrid PV/diesel/battery in hybrid electric ship system," *Journal of Operation and Automation in Power Engineering*, vol. 7, no. 1, pp. 16–26, May 2019.
- [17] S. Balderrama, F. Lombardi, F. Riva, W. Canedo, E. Colombo, and S. Quoilin, "A two-stage linear programming optimization framework for isolated hybrid microgrids in a rural context: The case study of the "El Espino" community," *Energy*, vol. 188, pp. 116073, Dec. 2019.
- [18] M. H. Shams, H. Niaz, J. Na, A. Anvari-Moghaddam, and J. J. Liu, "Machine learning-based utilization of renewable power curtailments under uncertainty by planning of hydrogen systems and battery storages," *Journal of Energy Storage*, vol. 41, pp. 103010, Sep. 2021.
- [19] P. Hou, P. Enevoldsen, J. Eichman, W. H. Hu, M. Z. Jacobson, and Z. Chen, "Optimizing investments in coupled offshore wind -electrolytic hydrogen storage systems in Denmark," *Journal of Power Sources*, vol. 359, pp. 186–197, Aug. 2017, doi: 10.1016/j.jpowsour.2017.05.048.
- [20] W. P. Zhang, A. Maleki, M. A. Rosen, and J. Q. Liu, "Sizing a stand-alone solar-wind-hydrogen energy system using weather forecasting and a hybrid search optimization algorithm," *Energy Conversion and Management*, vol. 180, pp. 609–621, Jan. 2019.
- [21] L. B. Jaramillo and A. Weidlich, "Optimal microgrid scheduling with peak load reduction involving an electrolyzer and flexible loads," *Applied Energy*, vol. 169, pp. 857–865, May 2016.
- [22] V. N. Dinh, P. Leahy, E. McKeogh, J. Murphy, and V. Cummins, "Development of a viability assessment model for hydrogen production from dedicated offshore wind farms," *International Journal of Hydrogen Energy*, vol. 46, no. 48, Jul. 2021, doi: 10.1016/j.ijhydene.2020.04.232.
- [23] S. H. Pishgar-Komleh, A. Keyhani, and P. Sefeedpari, "Wind speed and power density analysis based on Weibull and Rayleigh distributions (a case study: Firuzkooh county of Iran)," *Renewable and Sustainable Energy Reviews*, vol. 42, pp. 313–322, Feb. 2015.
- [24] R. Hosseinalizadeh, H. Shakouri G, M. S. Amalnick, and P. Taghipour, "Economic sizing of a hybrid (PV-WT-FC) renewable energy system (HRES) for stand-alone usages by an optimization-simulation model: Case study of Iran," *Renewable and Sustainable Energy Reviews*, vol. 54, pp. 139–150, Feb. 2016.

- [25] A. Buttler and H. Spliethoff, "Current status of water electrolysis for energy storage, grid balancing and sector coupling via power-to-gas and power-to-liquids: A review," *Renewable and Sustainable Energy Reviews*, vol. 82, pp. 2440–2454, Feb. 2018.
- [26] J. Brauns and T. Turek, "Alkaline water electrolysis powered by renewable energy: A review," *Processes*, vol. 8, no. 2, pp. 248, Feb. 2020.
- [27] P. Olivier, C. Bourasseau, and P. B. Bouamama, "Low-temperature electrolysis system modelling: A review," *Renewable and Sustainable Energy Reviews*, vol. 78, pp. 280–300, Oct. 2017.
- [28] D. M. See and R. E. White, "Temperature and concentration dependence of the specific conductivity of concentrated solutions of potassium hydroxide," *Journal of Chemical & Engineering Data*, vol. 42, no. 6, pp. 1266–1268, Nov. 1997.
- [29] Ø. Ulleberg, "Modeling of advanced alkaline electrolyzers: A system simulation approach," *International Journal of Hydrogen Energy*, vol. 28, no. 1, pp. 21–33, Jan. 2003.
- [30] M. Sánchez, E. Amores, L. Rodríguez, and C. Clemente-Jul, "Semi-empirical model and experimental validation for the performance evaluation of a 15 kw alkaline water electrolyzer," *International Journal of Hydrogen Energy*, vol. 43, no. 45, pp. 20332–20345, Nov. 2018.
- [31] Z. Abdin, C. Webb, and E. M. Gray, "Modelling and simulation of an alkaline electrolyser cell," *Energy*, vol. 138, pp. 316–331, Nov. 2017.
- [32] C. H. Li, X. J. Zhu, G. Y. Cao, S. Sui, and M. R. Hu, "Dynamic modeling and sizing optimization of stand-alone photovoltaic power systems using hybrid energy storage technology," *Renewable Energy*, vol. 34, no. 3, pp. 815–826, Mar. 2009.
- [33] J. Andersson and S. Grönkvist, "Large-scale storage of hydrogen," *International Journal of Hydrogen Energy*, vol. 44, no. 23, pp. 11901–11919, May 2019.
- [34] K. Deb, A. Pratap, S. Agarwal, and T. Meyarivan, "A fast and elitist multiobjective genetic algorithm: NSGA-II," *IEEE Transactions on Evolutionary Computation*, vol. 6, no. 2, pp. 182–197, Apr. 2002.
- [35] S. R. Salkuti, "Day-ahead thermal and renewable power generation scheduling considering uncertainty," *Renewable Energy*, vol. 131, pp. 956–965, Feb. 2019, doi: 10.1016/j.renene.2018.07.106.
- [36] A. Turk, Q. W. Wu, M. L. Zhang, and J. Østergaard, "Day-ahead stochastic scheduling of integrated multi-energy system for flexibility synergy and uncertainty balancing," *Energy*, vol. 196, pp. 117130, Apr. 2020, doi: 10.1016/j.energy.2020.117130.
- [37] U. Akram, M. Khalid, and S. Shafiq, "Optimal sizing of a wind/solar/battery hybrid grid-connected microgrid system," *IET Renewable Power Generation*, vol. 12, no. 1, pp. 72–80, Jan. 2018.
- [38] A. Ursúa, L. Marroyo, E. Gubía, L. M. Gandía, P. M. Diéguez, and P. Sanchis, "Influence of the power supply on the energy efficiency of an alkaline water electrolyzer," *International Journal of Hydrogen Energy*, vol. 34, no. 8, pp. 3221–3233, May 2009.
- [39] J. Rodríguez and E. Amores, "CFD modeling and experimental validation of an alkaline water electrolysis cell for hydrogen production," *Processes*, vol. 8, no. 12, pp. 1634, Dec. 2020.
- [40] W. Wei and J. H. Wang, *Modeling and Optimization of Interdependent Energy Infrastructures*, Switzerland: Springer, 2020.
- [41] European Commission. (2019, Oct.). Photovoltaic geographical information system. [Online]. Available: <https://re.jrc.ec.europa.eu>
- [42] Nord Pool. [Online]. Available: <https://www.nordpoolgroup.com/>



Shi You received the M.Sc. degree in Electrical Engineering from the Chalmers Institute of Technology, Gothenburg, Sweden, in 2007, and the Ph.D. degree in Electrical Engineering from the Technical University of Denmark (DTU), Denmark, in 2011. He is currently a Senior Researcher with the Center for Electric Power and Energy, Department of Electrical Engineering, DTU. His research interests include optimal design, planning, operation and control of distributed energy resources, active distribution networks, and integrated multi-carrier energy systems.



Marie Münster is Professor in Energy System Modeling at the Technical University of Denmark. She holds an M.Sc. degree in Energy Planning and a Ph.D. degree in Energy Modeling. She has extensive experience within the field of energy system modeling with focus on integrated energy systems and smart sector coupling analyzing technologies producing power, heat, gas and transport fuels (including PtX). She has been project leader and WP lead on several Danish and international research projects.



Henrik W. Bindner received the M.Sc. degree in Electrical Engineering from Technical University of Denmark, Denmark (DTU), in 1988. Since 1990 he has been with DTU where he currently is a research group leader at Center for Electric Power and Energy Part of Department of Electrical Engineering. He has been working on research projects in the field of smart grids, intelligent, integrated multi-energy systems. He has been a lead developer of the multi-energy research facility SYS-LAB/PowerlabDK. He has participated in several European research projects in the fields as work package leader and in many Danish projects as principal investigator and main contributor. He has supervised more than 20 PhDs covering different aspects of modelling, control and management of smart grid and integrated energy systems. He is sub-program leader in EERA JP Smart Grids and co-task lead in Mission Innovation IC#1 on smart grids.



Yi Zheng received the B.S. and M.S. degrees in Thermal Engineering from Tsinghua University, Beijing, China, in 2016 and 2018, respectively. He is currently a Ph.D. student from the Technical University of Denmark (DTU). His research interests include the modeling, optimal planning and operation, techno-economic analysis of hydrogen energy systems and power-to-X systems.